Single-center approach for photodetachment and radiative electron attachment: Comparison with other theoretical approaches and with experimental photodetachment data

Miguel Lara-Moreno, Thierry Stoecklin, Philippe Halvick, Jean-Christophe J.-C. Loison

Single-center approach for photodetachment and radiative electron attachment: Comparison with other theoretical approaches and with experimental photodetachment data

Miguel Lara-Moreno, Thierry Stoecklin,* Philippe Halvick, and Jean-Christophe Loison
Université de Bordeaux, ISM, UMR 5255, 33405, Talence, France

(Received 11 January 2019; published 15 March 2019)

A single-center method for calculating photodetachment cross section for anions and radiative electron attachment cross section for neutral molecules by microreversibility is presented. It uses the integral equation method to calculate the ejected electron's continuum wave function while the single-electron bound function of the anion is described by the Dyson orbital. It is compared with related theoretical approaches and benchmarked to the experimental photodetachment cross sections of O_2^-, OH^-, and CN^-. The use of the plane-wave approximation of the ejected electron wave function combined with the Hartree-Fock frozen-core approximation of the Dyson orbital is also considered and its results are compared with those of our methods and with experiment. A good agreement between the calculated photodetachment cross sections and the experimental data is obtained for O_2^- and CN^- when using the three methods. For OH^-, the calculated scattering-wave electron photodetachment cross sections agree well with two most recent sets of experimental data among the three available while the plane-wave results disagree with all the experimental and theoretical data. The different approaches to calculate the Dyson orbital are also discussed as well as the convergence of the calculations with respect to the choice of the one-electron basis set. The approximation of Dyson orbitals by Kohn-Sham orbitals appears to overestimate the photodetachment cross section.

DOI: 10.1103/PhysRevA.99.033412

I. INTRODUCTION

The formation and destruction of anions in space [1] is a field of recent interest as, so far, only six molecular carbon chain anions (C_4H^-, C_6H^-, C_8H^-, CN^-, C_3N^-, C_5N^-) have been detected in the interstellar medium (ISM) [2–7]. They were seen in different carbon-rich sources, e.g., the carbon star IRC+10216 and the molecular cloud TMC1. As suggested by Herbst [8] long ago, radiative electron attachment (REA) could be a significant production mode of anions in these environments where the density of electron is relatively important (10^{-7} the density of H_2 which is typically ranging between 10^5 to 10^6 molecules cm^{-3} [9]). Such a value of the electron density is considered to be high as it is several orders of magnitude larger than the one of all the detected anions (around 10^{-11} the density of H_2) and leads to high electronic dissociative recombination fluxes which are considered to initiate the dense molecular clouds chemistry. Statistical calculations of the rate coefficients for REA to linear carbon chains C_n (n = 4–9), and C_nH (n = 2–8) have been reported [10,11]. It was shown that the REA rate coefficient increases strongly with the size of the molecule, mainly because the statistical autodetachment rate of the activated anionic complex is inversely proportional to the size of the phase space. More recently, accurate quantum calculations of the REA rate coefficients [12–14] have been performed for $C_{2n+1}N$ (n = 0,1,2) and $C_{2n}H$ (n = 1,2). These calculations were performed with rigid molecules, except for CN where the contribution of the vibrational relaxation process to REA was found to be negligible. The quantically calculated rate coefficients were found much smaller than the corresponding statistical rates and also too small to explain the observed abundance of anions in the ISM. However, electron attachment resonances are expected to enhance the REA rate coefficients. A detailed review of the studies of such mechanisms has been given by Millar *et al.* [1]. The possibility of dipole-bound states acting as doorway for REA via Feshbach resonances lying in the continuum of the anion has been investigated [15–17], as well as shape resonance due to electron attachment in π^* orbital for linear carbon chain with filled π bonding [18,19] or in cyanopolyyne [20], or shape resonance followed by IVR [21]. Long-lived activated anionic complex such as SF_6^{-*} and NC_4N^{-*} have been observed experimentally [22,23]. Metastable states with long lifetime are expected to enhance REA.

On the experimental side, measurements of REA cross sections are scarce due to the difficulties of measuring these very low-magnitude cross sections and also to avoid a collisional stabilization before the slow radiative emission. Conversely, the reverse process (electron photodetachment from anions) has been the subject of many studies. Furthermore, experimental data are available for the latter process for several diatomic anions, thus allowing to benchmark our theoretical results. On the theoretical side, the first methods which apply equivalently to REA and electron photodetachment (EPD) were proposed in [24] and were based on the use of first Born approximation. These approaches rely on the fact that for nonpolar systems, the long-range interaction potential between the leaving or impinging electron and the neutral molecule is negligible, thus allowing the use of a plane wave for describing the electron wave function. Within this one-

*thierry.stoecklin@u-bordeaux.fr

electron approach, the wave function of the departing electron inside the anion is considered to be the highest occupied molecular orbital (HOMO). This approach was revisited more recently by several authors who improved this treatment by taking into account the electronic correlation and relaxation of the molecular target through the use of the Dyson orbital calculated from coupled-cluster method [25] or from density functional theory (DFT) [26]. The use of a computed scattering wave function instead of a plane wave for the motion of the electron in the continuum was also considered very early in the field of molecular photoionization [27] but its first use for EPD was only proposed in 2013 [28] for CN^- within the complex Kohn variational formalism. We present here a similar approach than this later study, but use instead the integral equation formalism [29] to obtain the scattered electron wave function.

The paper is organized as follows. In Sec. II are given the main steps of the scattering method used as well as the description of the calculation of the Dyson orbitals. The parameters of the different calculations are given in Sec. III and a first test of the method is presented in Sec. IV which reports the calculation of the EPD applied to $O_2{}^-$, CN^-, and OH^-, along with a comparison to the available experimental data and to the other theoretical results obtained by the Kohn variational principle and the *R*-matrix method. In the second part of this section, the plane-wave approximation is used to investigate the convergence of the REA and EPD cross sections as a function of the size and type of the one-electron basis set as well as different approximations for the calculation of the Dyson orbital. The conclusions of this study are presented in Sec. V.

II. THEORY

In this section we give a brief account of the method used to calculate the EPD and REA cross sections for linear molecules. This method can be straightforwardly extended to treat nonlinear molecules as well. It relies on a single-center body-fixed expansion of the electronic bound state and continuum wave around the center of mass of the molecule.

For a given value of the initial relative angular momentum l_0 and its projection Λ along the linear target molecule axis, one writes the scattered electron wave function such as

$$\psi^{\rm Scat}_{\Lambda l_0}(\vec{r}) = \frac{1}{r}\sum_{l} \Upsilon^{\rm Scat}_{\Lambda l_0,l}(r) Y_l^{\Lambda}(\hat{r}). \tag{1}$$

In a similar way, the single-electron wave function of the anion is taken to be a Dyson orbital also expanded in spherical harmonics,

$$\psi^{\rm Dyson}_{\Lambda'}(\vec{r}) = \sum_{l'} \Upsilon^{\rm Dyson}_{\Lambda',l'}(r) Y_{l'}^{\Lambda'}(\hat{r}), \tag{2}$$

where Λ' is the projection of the electronic angular momentum l' of the anion along its molecular axis.

A. REA and EPD cross sections

The expressions of the cross section as a function of the dipole moment matrix elements were given long ago for the photoionization of neutral molecules [27] or for the EPD of anions [30]. While the same expression is used for these two processes, the departing electron is subjected to potentials which differ strongly in strength and range. The cross section for EPD is

$$\sigma_{\rm EPD}(\omega) = \frac{4\pi^2\omega}{9c}\sum_{l_0\Lambda}\left[\mu_{l_0}^{\Lambda\Lambda'}\right]^2, \tag{3}$$

where

$$\mu_{l_0}^{\Lambda\Lambda'} = N_0^{\frac{1}{2}}\left\langle \psi^{\rm Scat}_{\Lambda l_0}\middle|\mu_\pi\middle|\psi^{\rm Dyson}_{\Lambda'}\right\rangle \tag{4}$$

are the dipole matrix elements, N_0 is the degeneracy factor (see below Sec. III C), ω is the photon frequency, c the speed of light, and μ_π the components of the dipole moment with $\pi \in \{-1, 0, 1\}$.

Using Eqs. (1) and (2), the expression (4) can be rewritten

$$\mu_{l_0}^{\Lambda\Lambda'} = \sum_{l,l'} I_{ll'}^{\Lambda\Lambda'}\int_0^\infty dr\, \Upsilon^{\rm Scat}_{\Lambda l_0,l}(r) r^3 \Upsilon^{\rm Dyson}_{\Lambda',l'}(r) \tag{5}$$

with

$$I_{ll'}^{\Lambda\Lambda'} = (-)^{\Lambda}\sqrt{(2l+1)(2l'+1)}\begin{pmatrix} l & 1 & l' \\ 0 & 0 & 0\end{pmatrix} \times \begin{pmatrix} l & 1 & l' \\ -\Lambda & \pi & \Lambda'\end{pmatrix} \tag{6}$$

which has a nonzero value only if $\pi = \Lambda - \Lambda'$.

The cross section for REA, which is the reverse process of EPD, is straightforwardly obtained by microscopic reversibility [31]:

$$\sigma_{\rm REA}(E_e) = \left(\frac{g_{\rm anion}}{g_{\rm neutral}}\right)\frac{\hbar^2\omega^2}{2m_eE_ec^2}\sigma_{\rm EPD}(\omega), \tag{7}$$

where the quantities $g_{\rm neutral}$ and $g_{\rm anion}$ are the statistical weights of the electronic states of the neutral molecule and of the anion, respectively, E_e is the electron kinetic energy, and m_e is the electron mass. Let us note that this principle of microreversibility should be applied to processes with well-specified internal quantum states (rotational, vibrational, electronic) of the initial and final species. Since in this work we are not considering the rovibrational states of the anion and of the neutral molecule, the use of Eq. (7) is an approximation.

We will now detail the procedures used for obtaining the radial coefficients $\Upsilon^{\rm Dyson}_{\Lambda',l'}$ and $\Upsilon^{\rm Scat}_{\Lambda l_0,l}$ of the Dyson orbital and of the scattering wave function, respectively, in Secs. II B and II C.

B. Calculation of the Dyson orbital

Let us consider an N-electron molecular system, neutral or anionic, represented by the electronic wave function $\psi^N(\vec{r}_1, \vec{r}_2, \ldots, \vec{r}_N)$. After ionization or electron detachment, this system has lost one electron and its $(N-1)$-electron wave function is represented by $\psi^{N-1}(\vec{r}_1, \vec{r}_2, \ldots, \vec{r}_{N-1})$. The Dyson orbital is then defined by the $(N-1)$-dimensional integral

$$\psi^{\rm Dyson}(\vec{r}) = \sqrt{N}\int \psi^{N-1}(\vec{r}_1, \ldots, \vec{r}_{N-1}) \times \psi^N(\vec{r}_1, \ldots, \vec{r}_N) d\vec{r}_1 \ldots d\vec{r}_{N-1}. \tag{8}$$

TABLE I. Basis set used in this work.

Type	Basis	H	B–Ne
GTO	aug-cc-pVQZ	$[5s4p3d2f]$	$[6s5p4d3f2g]$
GTO	aug-cc-pV5Z	$[6s5p4d3f2g]$	$[7s6p5d4f3g2h]$
GTO	aug-cc-pV6Z	$[7s6p5d4f3g2h]$	$[8s7p6d5f4g3h2i]$
GTO	aug-cc-pV6Z++	$[9s8p5d4f3g2h]$	$[10s9p6d5f4g3h2i]$
STO	VB2	$4s2p1d$	$6s4p2d1f$
STO	VB3	$5s3p2d1f$	$7s5p3d2f1g$

If ψ^N and ψ^{N-1} are represented by accurate multiconfigurational wave functions, then the Dyson orbital gathers the effects of electronic correlation on both systems and therefore the effects of the electronic relaxation which results from the addition or subtraction of one electron in the molecular electronic wave function.

A method for computing the Dyson orbital from multiconfigurational self-consistent field (MCSCF) wave functions is detailed in the Appendix. It is based on the overlaps between the orbitals of the N-electron system and the orbitals of the $(N-1)$-electron system. Other *ab initio* methods have been reported, using the equation-of-motion coupled-cluster method [25] (EOM-CCSD) or the construction of a biorthonormal set of two multiconfigurational wave functions [32].

The calculated Dyson orbital is then conveniently represented by an expansion over the molecular orbital set of the N-electron system

$$\psi^{\text{Dyson}}(\vec{r}) = \sum_p b_p \phi_p(\vec{r}), \tag{9}$$

where the index p runs over all occupied molecular orbitals.

A simple approximation of the Dyson orbital is given by the Hartree-Fock (HF) frozen-core (FC) approach [24,27]. Within this approximation, the HF orbitals of the anion are used to describe those of the remaining neutral core. In that case, the integral (8) is easily calculated. The Dyson orbital is just the spatial orbital from which the electron is ejected. This approximation neglects the electronic correlation and the relaxation of the molecular orbitals after the photodetachment.

Kohn-Sham (KS) orbitals have been recently proposed as good candidates for approximating the Dyson orbital [26,33,34]. Although KS orbitals were introduced as a mere artifact only for calculating the total energy and charge density, the latter proposition is based on the analogies found between Dyson's quasiparticle and KS equations.

In any case, the Dyson orbital is represented as a linear combination of either Gaussian (GTO) or Slater (STO) type orbitals. The radial expansion coefficients (2) are determined from a set of analytical relations expressed in terms of modified Bessel functions [35,36]. The different basis sets [37,38] used in this work are detailed in Table I.

C. Calculation of the electron's continuum wave function

1. Scattered wave

In this section we present our adaptation to EPD and REA of the integral equations approach developed long ago by Rescigno and Orel [29,39] for electron–molecule collisions. While only the main steps of the implementation of the method for linear molecules will be presented, more details can be found in the seminal references [29,39] and in some of our previous works [40]. First, the electronic wave function of the target is analytically expanded in symmetrized spherical harmonics and the expansion coefficients are utilized to obtain the static interaction potential with the impinging or leaving electron. More specifically, we will consider here an MCSCF wave function and use the natural orbitals and their occupancies to obtain this contribution. The method also entails obtaining a diagonal separable form of the exchange potential kernel for the lowest symmetries Σ, Π, and Δ of the scattered electron wave function in the same atomic orbital basis set than the one used for the Dyson orbital, possibly augmented of a few functions centered around the center of mass

$$K(r, r') = \sum_\alpha \chi_\alpha(r)\xi_\alpha\chi_\alpha(r'), \tag{10}$$

where ξ_α and $\chi_\alpha(r)$ are, respectively, the eigenvalues and eigenvectors of the exchange kernel represented in the atomic orbital basis set. If needed, a density functional Hara's free-electron-gas exchange potential [41] (HFEGE) is used for the higher symmetries. A density functional form of the correlation-polarization potential, as introduced by Padial and Norcross [42], is also obtained from the same electronic wave function and included in the local interaction potential. The scattering wave function is expanded in spherical harmonics and the resulting single-center coupled equations for the radial components of the scattering wavefunction take the usual form

$$\left(\frac{d^2}{dr^2} - \frac{l(l+1)}{r^2} + k^2\right)\Phi_{ll_0}(r) = \sum_{l'}\left[U_{ll'}(r)\Phi_{l'l_0}(r) + \sum_\alpha \chi_\alpha^l(r)\xi_\alpha \int_0^\infty dr' \chi_\alpha^{l'}(r')\Phi_{l'l_0}(r')\right],$$

where, to make the notation less cluttered, the projection Λ of the relative angular momentum associated with the symmetry for which the calculations are performed is not mentioned. In this expression, $U_{ll'}$ denotes the matrix elements of the local contributions to the interaction potential which include the static and correlation-polarization potentials. The integral form of these equations is solved with the Sams and Kouri method [43,44] extended by Rescigno and Orel to the multichannel case for a separable exchange potential [29,39]. The radial components of the wave function are expressed as a linear combination of homogeneous and inhomogeneous terms

$$\Upsilon^{\text{Scat}}_{\Lambda l_0, l}(r) \equiv \Phi_{ll_0}(r) = \Phi^0_{ll_0}(r) + \sum_\alpha \Phi^\alpha_l(r) C^\alpha_{l_0} \tag{11}$$

which both satisfy a set of Volterra equations, which are for the homogeneous term

$$\Phi^0_{ll_0}(r) = \delta_{ll_0} j_l(kr) + \sum_{l'} \int_0^r dr' g_l(r, r') U_{ll'}(r') \Phi^0_{l'l_0}(r') \tag{12}$$

and for the inhomogeneous term

$$\Phi_l^\alpha(r) = \int_0^r dr' g_l(r,r')\chi_\alpha^l(r') + \sum_{l'}\int_0^r dr' g_l(r,r')U_{ll'}(r')\Phi_{l'}^\alpha(r'). \quad (13)$$

The integral equations algorithm is very efficient but requires the use of two kinds of well-documented stabilization methods [29] corresponding to a change of the initial conditions. The upper triangular stabilization (UTS) entails decomposing the homogeneous solution, at some given propagation distance, into the product of the upper and lower triangular matrices. The solution matrix is replaced by the resulting upper triangular matrix whose columns are guaranteed to be linearly independent. The second kind of stabilization, referred to as *physical* by its authors [29], is designed to make the solution matrix resemble the physical solution as much as possible. In both kinds, the stabilization of the homogeneous part of the solution can be written in terms of a transformation matrix **T** such that

$$\Phi_{ll_0}^0 \to \tilde{\Phi}_{ll_0}^0 = \sum_k \Phi_{lk}^0 T_{kl_0}. \quad (14)$$

For the same value of the propagation distance, an associated stabilization of the inhomogeneous part of the scattering wave function needs also to be performed. Again, it can be written for both kinds of stabilization method in terms of a transformation matrix **d** and the stabilized homogeneous part of the wave function:

$$\Phi_l^\alpha \to \tilde{\Phi}_l^\alpha = \Phi_l^\alpha + \sum_{l''}\tilde{\Phi}_{ll''}^0 d_{l''}^\alpha. \quad (15)$$

The wave function is propagated outwardly and stabilized regularly up to the asymptotic region where the boundary conditions are applied. The reactance matrix and the elastic cross section are then extracted.

If we now apply this method to the propagation of the dipole moment matrix elements defined in Eq. (4), we see that the two terms of the electron's continuum wave function [Eq. (11)] need to be taken into account. Thus, the dipole moment matrix elements can be split into two contributions, associated with the local and nonlocal parts of the interaction potential, which are, respectively, referred to as the static and exchange contributions

$$\mu_{l_0}^{\Lambda\Lambda'} = \left[\mu_{l_0}^{\Lambda\Lambda'}\right]_{\rm Stat} + \left[\mu_{l_0}^{\Lambda\Lambda'}\right]_{\rm Exc}, \quad (16)$$

where the static contribution is

$$\left[\mu_{l_0}^{\Lambda\Lambda'}\right]_{\rm Stat} = \sum_{l,l'} I_{ll'}^{\Lambda\Lambda'}\int_0^\infty r^3\Phi_{ll_0}^0(r)\Upsilon_{\Lambda',l'}^{\rm Dyson}(r)dr \quad (17)$$

and the exchange contribution is

$$\left[\mu_{l_0}^{\Lambda\Lambda'}\right]_{\rm Exc} = \sum_\alpha C_{l_0}^\alpha M_\alpha^{\Lambda\Lambda'}, \quad (18)$$

where

$$M_\alpha^{\Lambda\Lambda'} = \sum_{l,l'} I_{ll'}^{\Lambda\Lambda'}\int_0^\infty r^3\Phi_l^\alpha(r)\Upsilon_{\Lambda',l'}^{\rm Dyson}(r)dr. \quad (19)$$

These two contributions are accumulated along the propagation of the continuum wave function and then need also to be stabilized at the points where the wave function is stabilized.

We obtain straightforwardly from Eq. (14) that the stabilization procedure of the homogeneous part of the dipole matrix is simply given by

$$\left[\mu_{l_0}^{\Lambda\Lambda'}\right]_{\rm Stat} \to \left[\tilde{\mu}_{l_0}^{\Lambda\Lambda'}\right]_{\rm Stat} = \sum_k T_{kl_0}\left[\mu_k^{\Lambda\Lambda'}\right]_{\rm Stat} \quad (20)$$

while using Eq. (15), the corresponding transformation of the exchange part of the dipole matrix is found to be for the intermediary matrix **M**:

$$M_\alpha^{\Lambda\Lambda'} \to \tilde{M}_\alpha^{\Lambda\Lambda'} = M_\alpha^{\Lambda\Lambda'} + \sum_{l''} d_{l''}^\alpha\left[\tilde{\mu}_{l''}^{\Lambda\Lambda'}\right]_{\rm Stat}. \quad (21)$$

2. Plane-wave approximation

We have also applied the first Born approximation to the REA and EPD problems as it is very simple to use and allows huge computer time saving since neither the electron-molecule interaction potential nor the scattering wave function need to be calculated. Indeed, within the first Born approximation, the scattering wave function is just a plane wave and the interaction potential between the impinging electron and the target is then implicitly considered to be zero. This is a reasonable approximation in the case of the interaction between an electron and a nonstrongly dipolar molecule which is relatively short ranged. The first implementation of the method for the EPD from anions was proposed long ago [24]. In this early attempt, the Dyson orbital was approximated by the HOMO of the anion. More recently, new implementations of the method using instead a Dyson orbital calculated by the DFT or coupled-cluster methods were shown to give very good results for several systems [26,45].

The expansion coefficients in spherical harmonics of the scattering wave function defined in Eq. (1) are easily obtained from

$$\psi_{\Lambda l_0}^{\rm Scat}(\vec{r}) = \sqrt{\frac{k}{(2\pi)^3}}e^{i\vec{k}\vec{r}} = \sqrt{\frac{k}{(2\pi)^3}}\sum_l i^l j_l(kr)P_l(\cos\theta). \quad (22)$$

The radial expansion coefficient $\Upsilon_{\Lambda l_0,l}^{\rm Scat}(r)$ of Eq. (1) is then in this case the Ricatti-Bessel functions.

III. PARAMETERS OF THE CALCULATIONS

All the calculations are performed using the following assumptions:

(i) The electron affinities, the ionization energies, the parallel and perpendicular polarizabilities of the neutral molecules are fixed to the values shown in Table II.

(ii) We consider only the contributions from the electronic ground states of both the anion and the neutral molecule to the REA or EPD processes.

TABLE II. Experimental bond length (r_e), Dipole moment (μ), polarizabilities (α), ionization energies (IE), and electron affinities (EA) used in the calculations. Dipole moments and polarizabilities were calculated using the finite field method implemented in MOLPRO at the CCSD(T)/aug-cc-pV6Z level.

Molecule	r_e (a_0)	μ (Debye)	$\alpha_\parallel$ (a_0^3)	$\alpha_\perp$ (a_0^3)	IE (eV)	EA (eV)
O_2	2.282	0	14.11	8.74	12.07 [46]	0.4480 [47]
CN	2.214	1.40	25.13	16.32	14.17 [48]	3.8620 [49]
OH	1.833	1.63	8.62	6.21	13.02 [50]	1.8277 [51]

A. Dyson orbital

Four approaches for calculating the Dyson orbital are compared: HF-FC, KS-B3LYP, EOM-CCSD, and the complete active-space self-consistent field (CASSCF) method with full valence active space. In the case of the HF-FC and KS-B3LYP methods, since CN^- and OH^- have a singlet ground state, the Dyson orbital is just the HOMO. For O_2^- which has a $^2\Pi$ ground state with the configuration π^3, and becomes after photodetachment the O_2 molecule with a $^3\Sigma^-$ ground state and the π^2 configuration, the Dyson orbital is the π orbital occupied by two electrons in the ground state of O_2^-.

The experimental equilibrium bond lengths of the anions are employed in the calculations, namely, 2.224, 2.551, 1.833 a_0 for CN^- [49], O_2^- [52], and OH^- [53], respectively. The maximum value of l' for the expansion [Eq. (2)] of the Dyson orbital in spherical harmonics is fixed to 35, 34, and 25 for CN, O_2, and OH, respectively.

All electronic calculations needed for the computation of the HF-FC, KS-B3LYP, and CASSCF Dyson orbitals were performed using the MOLPRO package [54] and the SMILES package [55]. The calculations of the EOM-CCSD Dyson orbitals were done with the Q-CHEM package [56]. In the latter calculations, a reduced aug-cc-pV6Z basis set without h and i shells was used, thus allowing a calculation of the EPD cross sections with the EZDYSON program [57]. For O_2^-, in order to compute the EOM-CCSD Dyson orbital in a reasonable amount of time and memory, the virtual space was reduced by 50 orbitals.

B. Continuum wave function

1. Scattered wave

In order to solve the integrodifferential equations detailed in Sec. II C, we need first to calculate the static, correlation-polarization, and exchange potentials.

(a) Static potential. The fundamental electronic wave functions of the CN, O_2, and OH molecules are described at the CASSCF level with full valence active space and using the basis set shown in Table I and the experimental geometries (Table II). A total of 150 values of l are included in the analytical expansions of the natural orbitals in spherical harmonics. We then use this expansion together with the natural orbital populations to obtain the 80 first terms of the static potential multipole expansion.

(b) Correlation-polarization potential. We use the local density functional form of Padiall and Norcross [42] and the polarizabilities given in Table II to obtain the $l = 0$ and 2 contributions included in our calculations.

(c) Exchange potential. Two kinds of exchange potential are employed. First, the local density functional Hara's free-electron-gas model [41] which is calculated for a maximum values of $l = 40$ and using the ionization energies given in Table II. Second, a nonlocal separable form [39] is computed for the Σ and Π symmetries in the Gaussian basis set which is used to calculate the electronic wave function. The maximum value of l considered for the expansion of the Gaussian functions is 80 for the three systems. For the Δ symmetry, a Hara's free-electron-gas potential is used as it was shown to give equivalent results.

2. Plane wave

In all calculations based on plane wave, the partial-wave expansion [Eq. (22)] was truncated at a maximum value of 40 Riccatti-Bessel functions.

C. Spin and electronic degeneracies

As in any scattering problem we need to average the cross section over all initial states and to sum it over all the final states. In the case of photodetachment or photoionization of a closed-shell system with no electronic degeneracy, the calculated cross section must be multiplied by 2 [27,57,58]. This results from the fact that the final state combines two electrons in two different orbitals and must be a singlet state. The spin of the electron ejected from the initial closed-shell system can be up or down. Both spin projections lead to the same cross section and we have to sum over these two cases. This applies to the photodetachment of $CN^-(X\,^1\Sigma^+)$ giving $CN(X\,^2\Sigma^+)$. Let us now consider the photodetachment from $OH^-(X\,^1\Sigma^+)$. The HOMO is a π orbital occupied by four electrons. The final state is $OH(X\,^2\Pi)$ with the π orbital occupied by three electrons. The ejected electron can be any of the four initial electrons occupying the HOMO. The total photodetachment cross section is then the sum of the four equivalent cross sections calculated by considering only one electron among the four available ones. Thus, we multiply the calculated cross section by 4. Finally, let us turn to the photodetachment from $O_2^-(X\,^2\Pi)$ which has a π HOMO occupied by three electrons. We consider only the final state $O_2(X\,^3\Sigma_g^-)$. The final π HOMO is occupied by two electrons and must be a triplet state. This requires two open shells. Let us denote by π_x and π_y the two degenerate orbitals which form the π orbital. The initial state has two electrons in the π_x or π_y orbital and one electron in the other degenerate orbital. The final state must have one electron in each π_x and π_y orbital. Therefore, there is only the possibility to eject an electron from the doubly occupied orbital. This case reduces to the case of a closed-shell system with no electronic degeneracy and, therefore, we multiply the calculated cross section by 2. Furthermore, we have to average the cross section over all initial states. The two initial degenerate states of $O_2^-(X\,^2\Pi)$ are equivalent (two electrons in π_x and one in π_y or the reverse). Therefore, the cross section of only one case needs to be calculated.

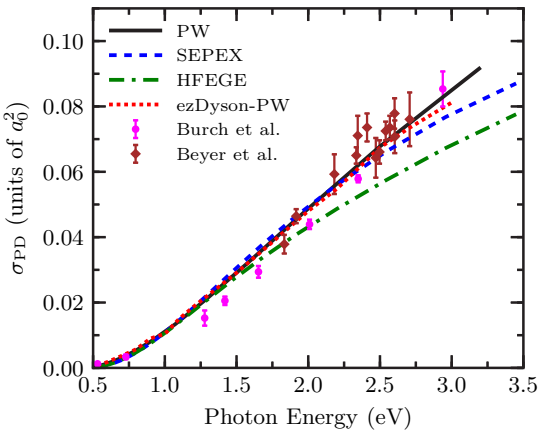

FIG. 1. Experimental [59,60] and calculated EPD cross section of O_2^-. The calculated cross sections correspond to the different representations of the electron continuum wave function: plane wave (PW), scattered wave using a separable exchange potential (SEPEX), scattered wave using Hara's free-electron-gas exchange potential (HFEGE). The dotted red line shows the PW cross section of Oana *et al.* [45].

IV. RESULTS

A. Comparison between theory and experiment

In this section we test our theoretical approaches by comparing the calculated EPD cross sections with the experimental data available for O_2^-, OH^- and CN^- in Figs. 1, 2, and 4, respectively. In these calculations the Dyson orbital as well as the different contributions to the interaction potential were calculated at the CASSCF level using the VB3 basis set.

For O_2^-, we see in Fig. 1 that there is a global good agreement between theory and experiment whatever the theoretical method used. The relatively good agreement between the scattered-wave and plane-wave calculations was expected as O_2 has no dipole. Therefore, the interaction potential between the ejected electron and O_2 is driven by the charge-quadrupole ($\propto r^{-3}$) and charge-induced dipole ($\propto r^{-4}$) interactions which are not very strong. Thus, the continuum wave function is well described by the plane-wave (PW) approximation for this system. The present PW cross section is in very good agreement with the PW cross section reported by Oana *et al.* [45], although both calculations use different basis sets and different methods for the calculation of the Dyson orbital. But, the EPD cross section of O_2^- is rather insensitive to the basis set, as shown in Sec. IV B. Furthermore, due to symmetry, the Dyson orbital is essentially the π_g orbital with a small contribution from the π_g^* orbital, therefore reducing the discrepancy which could come from the different methods of calculating the Dyson orbital.

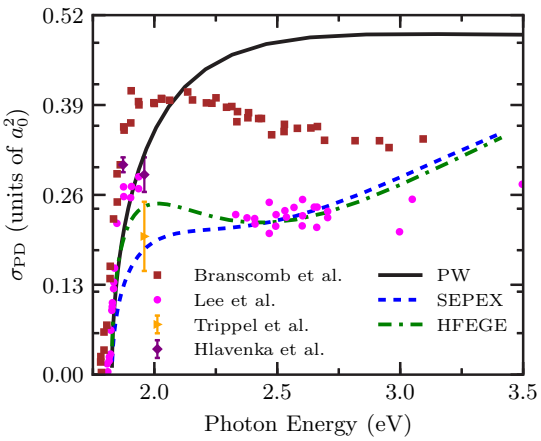

FIG. 2. Experimental [53,61–63] and calculated EPD cross section of OH^-. Notation as in Fig. 1.

In the case of OH^- represented in Fig. 2, four sets of experimental data are available which agree only for the lowest photon energies. At higher energy it becomes difficult to decide which set of experimental data are the most reliable. But, let us note that the experimental work of Branscomb *et al.* is the oldest one (1966) and gives the largest cross section while the work of Lee and Smith is more recent (1979) and is in good agreement with the most recent work of Hlavenka *et al.* (2009). In Branscomb's experiment, the anions were produced in discharge with a high degree of internal excitation, at an estimated temperature of ~850 K, while the later experiments were carried out between 8 and 300 K. Since the potential energy curves of OH and OH^- are very similar, the EPD cross section is not expected to be significantly affected by the vibrational excitation. Trippel *et al.* proposed that rotational excitation explains the larger cross section measured by Branscomb *et al.* but the cross section measured by Hlavenka *et al.* in the range 8–300 K shows no temperature dependence and, therefore, no rotational excitation dependence. More experimental data are necessary to understand this discrepancy.

Near the photodetachment threshold, the three sets of calculations describe reasonably well the increase of the cross section. At higher energy, a large discrepancy is observed between the PW cross section and the other two calculated cross sections which involve the calculation of the scattering wave function. This can be understood by reminding that OH is a strongly dipolar molecule and that, consequently, the interaction potential of this molecule with the ejected electron cannot be neglected. While the agreement between theory and experiment is not as good as for O_2^-, the set of experimental points of Lee and Smith [61] is, however, reasonably well reproduced by the SEPEX and HFEGE approaches, with a better match of the HFEGE approach which exhibits the low-energy bump observed in the experimental results. Among the three molecules considered in this study, OH^- is the one with the largest dipole moment. It is known that rotation should be taken into account in the case of strongly dipolar systems [64] whereas it is neglected within our approaches. However, EPD experiment [63] has shown there is no rotational dependence at temperature lower than 300 K. Several deficiencies of the first Born approximation are known, among which the nonorthogonality of the PW with the Dyson orbital is probably the most important one [24]. This later shortage is the most probable cause of the failure of the plane-wave approximation for this system.

A maximum is observed in the experimental and HFEGE photodetachment cross sections below 2 eV. This feature could indicate a resonance. However, the present calculations include only the fundamental electronic states of OH and

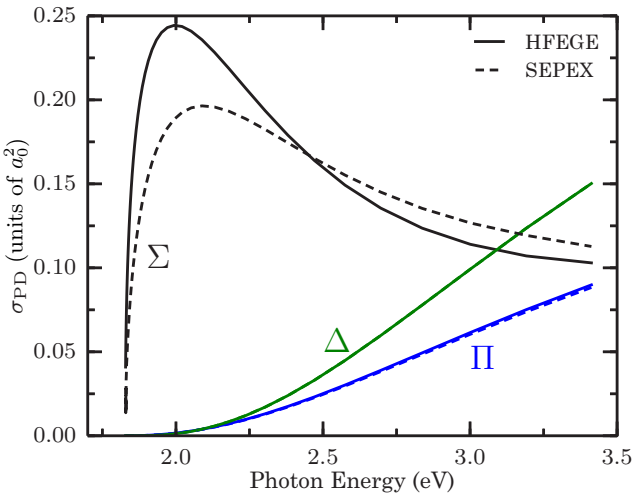

FIG. 3. Λ components of the EPD cross section of OH^-.

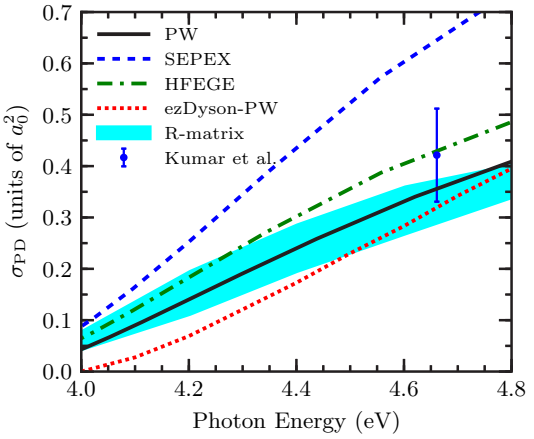

FIG. 4. Experimental [65] and calculated EPD cross section of CN^-. The cyan area corresponds to the *R*-matrix calculations of Khamesian *et al.* [13]. The dotted red line shows the PW calculation of Skomorowski *et al.* [20]. Notation as in Fig. 1.

OH^- and both rotation and vibration are neglected, thus only a shape resonance is possible. A check of the elastic cross section did not reveal any resonance. This is backed by the fact that some PW cross sections [24,26], for which no resonance is possible, also display the same maximum. If one assumes there is no resonance, what can cause the observed maximum? The partial-wave decomposition of the cross section gives the answer. At the photodetachment threshold energy, the cross section is proportional to $\Delta E^{l_{\min}+\frac{1}{2}}$ where ΔE is the excess energy above threshold and $l_{\min}$ the value of the lowest relative orbital angular momentum which contributes to the cross section [24]. In the case of OH^-, we have $l_{\min} = 0$, and therefore the cross section has an infinite slope at the threshold energy. As the energy increases, therefore increasing the relative orbital angular momentum, the $l = 0$ contribution decreases while the $l \geqslant 1$ contributions increase. Figure 3 shows the amplitude of the Λ components of the cross section (Λ is the projection of l on the internuclear axis). It appears clearly that the maximum of the cross section is a consequence of the early decrease of the $\Lambda = 0$ contribution above the 2-eV energy.

The calculated EPD cross sections for CN^- are compared in Fig. 4 to the single experimental point available. While the separable exchange cross section is too large, the PW and HFEGE results agree reasonably well with experiment, the HFEGE giving the best agreement. In order to assess the energy dependence of the cross section, we compared on the same figure our results with those obtained from state-of-the-art *R*-matrix calculation of Khamesian *et al.* [13]. Again, the agreement with our calculations is relatively good, especially for the plane wave and scattered wave using a HFEGE potential. The EPD cross section reported by Skomorowski *et al.* [20] for CN^-, calculated with the PW approximation, is slightly lower than the PW cross section of this work. There are at least three reasons for this discrepancy. First, Skomorowski *et al.* use a calculated value (3.99 eV) for the photodetachment threshold energy, while we use the experimental value, namely, 3.86 eV. The second origin of differences is the basis set. Skomorowski *et al.* use a GTO basis set while we use the VB3 STO basis set. As shown in Sec. IV B, the latter basis set gives larger cross sections than large GTO basis sets. Third, the cross section of Skomorowski *et al.* is based on EOM-CCSD Dyson orbitals while we use CASSCF Dyson orbitals.

There are unfortunately no experimental REA data for these three systems, but two sets of theoretical calculations are available for CN using the complex Kohn variational principle [28] and the *R*-matrix method [13]. The results of these calculations are compared with ours in Fig. 5. It can be seen that the cross sections calculated with a scattered wave agree quite well with the *R*-matrix and the Kohn variational principle results. Conversely, the plane-wave approximation does not reproduce the very low collision energy behavior. This result is understandable as the plane-wave approximation is expected to work well when the kinetic energy of the electron is large enough compared to the electron affinity of the target molecule. This suggests that the scattered wave should *in any case* be preferred for REA calculations at very low energy.

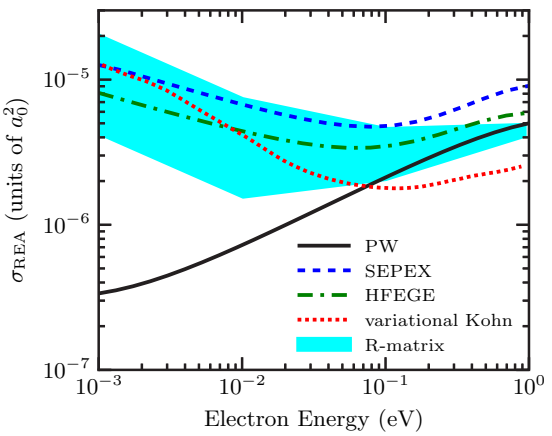

FIG. 5. Calculated REA cross section of CN^-. The cyan area corresponds to the *R*-matrix calculations of Khamesian *et al.* [13]. The dotted red line corresponds to the Kohn variational principle calculations of Douguet *et al.* [28]. Notation as in Fig. 1.

TABLE III. REA rate constant at 300 K for the different approaches discussed in the text. The notation $a(b)$ stands for $a \times 10^b$.

Molecule	SEPEX	HFEGE	PW	Herbst
O_2	6.1(−20)	7.1(−20)	5.1(−19)	2.0(−17)
CN	1.6(−15)	1.1(−15)	4.4(−16)	4.0(−18)
OH	4.8(−16)	6.8(−16)	6.8(−16)	1.1(−18)

We eventually calculated the REA rate constant at 300 K by Boltzman averaging of the SEPEX, HFEGE, and PW cross sections (see Table III). In the case of CN, the best agreement with the rate constant reported by Douguet *et al.* [28], 7×10^{-16} cm^3 molecule^{-1} s^{-1}, is obtained with the HFEGE and PW methods. The Douguet *et al.* results lie between the HFEGE and PW results. While not realistic at very low energy, the plane-wave approximation also appears to give the right order of magnitude of the REA rate constant at 300 K. It then offers a simple alternative in this temperature range for larger molecules for which the scattering-wave calculations could be time consuming. Also shown in Table III are the REA rate constants obtained using the statistical expression proposed by Herbst [8]. The statistical rate constants differ from our calculations by about two orders of magnitude. However, all calculations agree with the fact that the REA rate constants for diatomic molecules are particularly small.

B. Comparison of the methods and basis sets for the Dyson orbital evaluations

As seen above, there are several methods available to calculate the Dyson orbital and it is also necessary to select a one-electron basis set. In this section, we investigate how the REA and EPD cross sections are depending on the type and size of the one-electron basis set and also on the method used to calculate the Dyson orbital. We consider both Slater and Gaussian basis sets and apply the various approaches and basis sets to the three diatoms CN, O_2, and OH. As it was found in the previous section that the plane-wave approximation gives reasonable results for a low computation time, we decided to use this approximation to carry out this study.

Figure 6 shows first a comparison of the EPD cross sections obtained using different methods of electronic calculation for obtaining the Dyson orbital, all with the aug-cc-pV6Z basis set. The CASSCF approach is compared to the HF-FC, EOM-CCSD, and KS-B3LYP approaches. The EZDYSON program [57] was used to compute the cross sections from the EOM-CCSD Dyson orbitals. As it can be seen in this figure, the HF-FC approximation moderately underestimates the CASSCF cross sections as it neglects the electron correlation. In spite of this shortcoming, the HF-FC approach may offer a reliable first estimate of the EPD cross section when the size of the system prohibits the use the CASSCF approach. The EOM-CCSD approach gives larger cross sections than the CASSCF approach. Since the electronic correlation is accurately calculated by the EOM-CCSD method, this implies that the Dyson orbital calculated with this method has small contributions from many diffuse virtual molecular orbitals. This is expected to increase the EPD cross section. As a matter of fact, Fig. 6 shows that the discrepancy between both EOM-CCSD and CASSCF approaches is more or less proportional to the number of valence electrons

We also find that the KS-B3LYP calculation fail providing the right magnitude of the EPD cross section since it always overestimates its value. Since KS orbitals are proportional to the Dyson orbitals [33], one can understand why KS orbitals are able to reproduce relative measurements like momentum distributions while they fail estimating absolute values of the EPD cross section. This interpretation is confirmed by looking at the scaled KS results in Fig. 6, which reproduce correctly the energy dependence of the CASSCF EPD cross section.

We now focus our interest on the convergence of the EPD and REA results as a function of the size and the type of the one-electron basis set used to perform the computation of the Dyson orbital. These results are shown in Fig. 7, all calculated with the CASSCF method. The basis sets tested are those defined in Table I. The largest basis set, aug-cc-pV6Z++, corresponds to the aug-cc-pV6Z basis set augmented by a tempered set of two extra-diffuse functions for the s and p shells. The EPD cross section for O_2^- shows almost no variation with respect to the choice of the basis set. Conversely, the EPD cross sections for OH^- and CN^- show a significant dependence on the choice of the basis set. This can be understood by reminding that both OH and CN are polar molecules while O_2 is not. This means that the interaction between the scattered electron and CN or OH is more long ranged than for O_2. More diffuse functions are then required to describe properly the interaction of an electron with a polar molecule. This is indeed what can be seen in Fig. 7. The largest STO basis set give better results than the GTO ones since they are

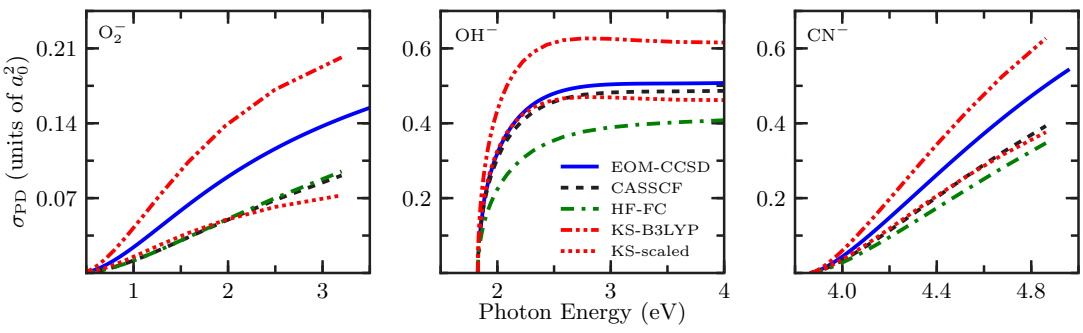

FIG. 6. Plane-wave EPD cross sections for different approaches to the calculation of the Dyson orbital.

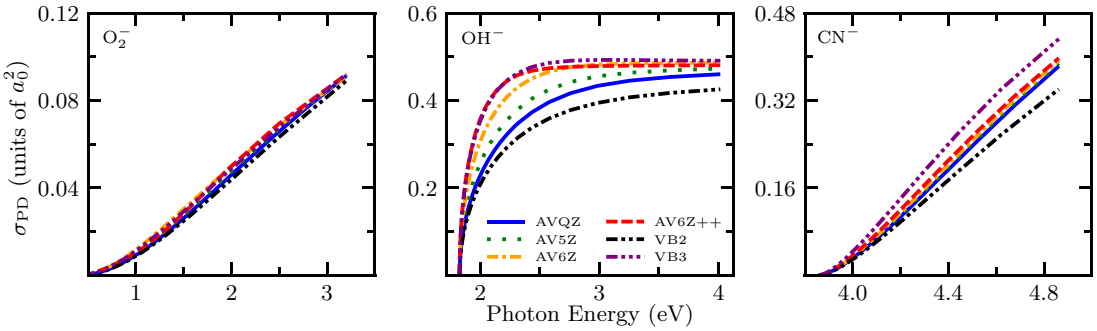

FIG. 7. Plane-wave EPD cross sections for different one-electron basis set employed in the CASSCF calculations of the Dyson orbital.

more diffuse. This is clearly seen when comparing the VB3 and aug-cc-pV6Z results in spite of the important difference of size between these two basis sets (Table I). Adding more diffuse functions to the large GTO basis set aug-cc-pV6Z does not change the EPD cross sections, except a small change for OH^- in the range 1.8–2.5 eV where the aug-cc-pV6Z++ cross section is closer to the VB3 cross section than to the aug-cc-pV6Z cross section. Since furthermore the STO orbitals reproduce accurately the cusp of the atomic orbitals, a smaller number of STO functions are sufficient to properly describe the Dyson orbital in the short-range region.

If we now compare in Fig. 8 the results obtained for the REA cross sections, we can see that only the low-energy regime is significantly dependent on the choice of the basis set. The explanation of this dependence is identical to the one we discussed for the EPD cross sections.

V. CONCLUSION

A method based on a body-fixed single-center approach and a variety of approximations of the Dyson orbital was presented for the calculation of the EPD and REA cross sections. Both the methods used to calculate the Dyson orbital and the scattering wave function were reviewed in detail. The methods were benchmarked by applying them to the three molecules CN, O_2, and OH for which experimental EPD data are available. The results of these approaches compare well with both experimental data and the only *R*-matrix and Kohn variational principle calculations available. We, however, expect that it may not be the case for strongly polar molecules as it is based on a body-fixed approach.

We also compared available REA and EPD data for these three systems with the results given by the combination of the use of the first Born approximation and the calculation of a Dyson orbital. For the systems where the dipole moment is not too large, and provided that the kinetic energy of the electron is large enough compared to the electron affinity of the target molecule in the case of REA calculations, we found that the plane wave is a good approximation of the scattering wave which furthermore reduces drastically computer time. This confirms the results of previous studies [24,26,45].

The plane-wave approximation was thus used to compare the results of several kinds of methods for the evaluation of the Dyson orbital which is a key ingredient in the calculation of EPD and REA cross sections. We find that KS-B3LYP results give the right energy dependence of the cross sections but overestimates the absolute magnitudes, while CASSCF and HF-FC give relatively close results. The effects of the size and type of orbital basis set was also investigated still with the plane-wave approximation. STO basis sets are found to perform better for a smaller number of basis functions than GTO basis sets. Among the three methods tested in this study, it is HFEGE scattering-wave approach developed in this work, which shows the best overall agreement with experiment. While less accurate, the plane-wave approximation combined with the use of HF-FC Dyson orbitals appears to be an efficient alternative tool for computing REA and EPD cross sections for large molecular systems with moderate dipole moment.

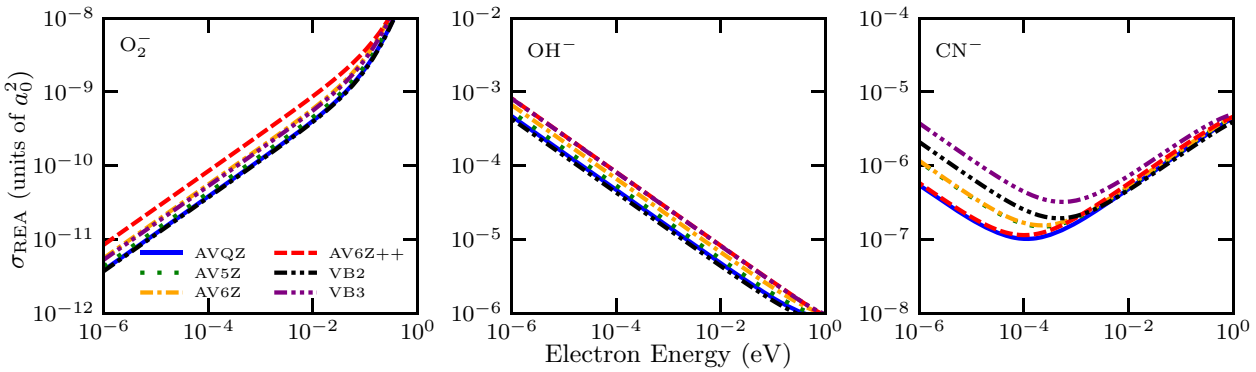

FIG. 8. Plane-wave REA cross section for different basis set employed in the CASSCF calculation of the Dyson orbital.

ACKNOWLEDGMENTS

We thank L. Truflandier for his valuable help in the DFT calculations. This research has been financially supported by the «Agence Nationale de la Recherche» (ANR-AnionCosChem project) and the French embassy in Cuba. Computer time for this study was provided by the Mésocentre de Calcul Intensif Aquitain computing facilities of Université de Bordeaux et Université de Pau et des Pays de l'Adour.

APPENDIX: DYSON ORBITAL CALCULATION

Let us consider a N-electron molecular system, neutral or anionic. After ionization or electron detachment, this system has lost one electron. If the electronic wave functions are expanded over a set of determinants, such as CASSCF or CI wave functions,

$$\Phi^N(x_1, x_2, \ldots, x_N) = \sum_{k=1}^{k_{\max}} C_k^N \Psi_k^N(x_1, x_2, \ldots, x_N), \tag{A1}$$

$$\Phi^{N-1}(x_1, x_2, \ldots, x_{N-1}) = \sum_{l=1}^{l_{\max}} C_l^{N-1} \Psi_l^{N-1}(x_1, x_2, \ldots, x_{N-1}), \tag{A2}$$

then the Dyson orbital [25,32,66] is defined by

$$\varphi^D(x_N) = \sqrt{N} \sum_{l=1}^{l_{\max}} C_l^{N-1} \sum_{k=1}^{k_{\max}} C_k^N \times \int dx_1 dx_2 \ldots dx_{N-1} \Psi_k^N(x_1, x_2, \ldots, x_N) \times \Psi_l^{N-1}(x_1, x_2, \ldots, x_{N-1}). \tag{A3}$$

We detail below how to calculate the $(N-1)$-dimensional integral, following closely Arbelo-González *et al.* [66].

Any N-electron Slater determinant can be rewritten as

$$\Psi_k^N(x_1, x_2, \ldots, x_N) = \frac{1}{\sqrt{N}} \sum_{i=1}^{N} (-)^{N+i} \psi_{ki}^{N-1}(x_1, x_2, \ldots, x_{N-1}) \chi_{d_{ki}}(x_N), \tag{A4}$$

where $\psi_{ki}^{N-1}(x_1, x_2, \ldots, x_{N-1})$ is the minor determinant obtained by removing the column i and the line N from the determinant $\Psi_k^N(x_1, x_2, \ldots, x_N)$, and where $\chi_{d_{ki}}$ is the molecular spin-orbital appearing at column i in determinant k. The spin-orbital number is given by the function d_{ki}. Using Eq. (A4), Eq. (A3) can be rewritten

$$\varphi^D(x_N) = \sum_{l=1}^{l_{\max}} C_l^{N-1} \sum_{k=1}^{k_{\max}} C_k^N \sum_{i=1}^{N} (-)^{N+i} \chi_{d_{ki}}(x_N) \times \int dx_1 dx_2 \ldots dx_{N-1} \Psi_l^{N-1}(x_1, x_2, \ldots, x_{N-1}) \times \psi_{ki}^{N-1}(x_1, x_2, \ldots, x_{N-1}). \tag{A5}$$

The summation on k runs on all determinants of the N-electron system, and the summation on i runs on all occupied spin orbitals of the determinant k. Thus, we can replace the summation on i by a summation on all spin orbitals of the N-electron system. Let us define the b coefficients such as

$$b_{d_{ki}} = \sum_{l=1}^{l_{\max}} C_l^{N-1} C_k^N (-)^{N+i} \times \int dx_1 dx_2 \ldots dx_{N-1} \Psi_l^{N-1}(x_1, x_2, \ldots, x_{N-1}) \times \psi_{ki}^{N-1}(x_1, x_2, \ldots, x_{N-1}), \tag{A6}$$

$$\varphi^D(x_N) = \sum_{k=1}^{k_{\max}} \sum_{i=1}^{N} b_{d_{ki}} \chi_{d_{ki}}(x_N). \tag{A7}$$

d_{ki} will run on all the spatial orbitals which are occupied at least one time in the list of the determinants. d_{ki} gives also the spin state. Thus, all the quantities $b_{d_{ki}}$ which belong to the same spatial orbital j and spin state σ can be summed and Eq. (A7) can be rewritten

$$\varphi^D(x_N) = \sum_{j=1}^{N_o} \sum_{\sigma=\alpha,\beta} b_{j\sigma} \chi_{j\sigma}(x_N), \tag{A8}$$

where N_o is the number of spatial orbitals (atomic or molecular).

The determination of the coefficients $b_{d_{ki}}$ involves the calculation of the $(N-1)$-dimensional integral

$$I_{lki} = \int dx_1 dx_2 \ldots dx_{N-1} \Psi_l^{N-1}(x_1, x_2, \ldots, x_{N-1}) \times \psi_{ki}^{N-1}(x_1, x_2, \ldots, x_{N-1}). \tag{A9}$$

The integral involves the product of two Slater determinants built over two nonorthogonal spin-orbital basis sets. The $(N-1)$-dimensional integral can be reorganized into an antisymmetrized product of $N-1$ one-dimensional integrals

$$I_{lki} = \sum_{p \in S_n} (-)^p \hat{\mathcal{P}} \int dx\, \varphi_{d_{l1}}(x) \chi_{d_{k1}}(x) \times \int dx\, \varphi_{d_{l2}}(x) \chi_{d_{k2}}(x) \ldots \times \int dx\, \varphi_{d_{l(i-1)}}(x) \chi_{d_{k(i-1)}}(x) \times \int dx\, \varphi_{d_{li}}(x) \chi_{d_{k(i+1)}}(x) \ldots \times \int dx\, \varphi_{d_{l(N-1)}}(x) \chi_{d_{kN}}(x), \tag{A10}$$

where the antisymmetrization operator acts over the $\chi_{d_{ki}}$ functions. This can be also written as a determinant in which appear the overlaps of every occupied molecular orbitals of the N-electron system with every occupied molecular orbitals of the $(N-1)$-electron system.

The functions $\varphi_{d_{lj}}$ and $\chi_{d_{ki}}$ are spin orbitals, i.e., the products of a spin function $\sigma \in [\alpha, \beta]$ and a spatial molecular orbital. The latter are expanded over the spatial atomic orbitals basis set. Let us recall that both N-electron and $(N-1)$-electron systems have the same atomic orbitals' basis set, the same geometry, but different molecular orbitals' basis sets. Therefore, the overlaps between spin orbitals appearing in Eq. (A10) are calculated with

$$\langle \varphi_{d_{li}} | \chi_{d_{kj}} \rangle = \delta_{\sigma_{d_{li}},\sigma_{d_{kj}}} \sum_{m=1}^{N_o} \sum_{n=1}^{N_o} u_{md_{li}} v_{nd_{kj}} S_{mn}, \qquad \text{(A11)}$$

where u and v are the LCAO coefficients and S the atomic orbital overlap matrix.

[1] T. J. Millar, C. Walsh, and T. A. Field, Chem. Rev. **117**, 1765 (2017).
[2] M. C. McCarthy, C. A. Gottlieb, H. Gupta, and P. Thaddeus, Astrophys. J. **652**, L141 (2006).
[3] J. Cernicharo, M. Guélin, M. Agúndez, K. Kawaguchi, M. McCarthy, and P. Thaddeus, Astron. Astrophys. **467**, L37 (2007).
[4] S. Brünken, H. Gupta, C. A. Gottlieb, M. C. McCarthy, and P. Thaddeus, Astrophys. J. **664**, L43 (2007).
[5] M. Agúndez, J. Cernicharo, M. Guélin, M. Gerin, M. C. McCarthy, and P. Thaddeus, Astron. Astrophys. **478**, L19 (2008).
[6] P. Thaddeus, C. A. Gottlieb, H. Gupta, S. Brünken, M. C. McCarthy, M. Agúndez, M. Guélin, and J. Cernicharo, Astrophys. J. **677**, 1132 (2008).
[7] J. Cernicharo, M. Guélin, M. Agúndez, M. C. McCarthy, and P. Thaddeus, Astrophys. J. **688**, L83 (2008).
[8] E. Herbst, Nature (London) **289**, 656 (1981).
[9] A. Bacmann, P. André, J.-L. Puget, A. Abergel, S. Bontemps, and D. Ward-Thompson, A&A **361**, 555 (2000).
[10] R. Terzevia and E. Herbst, Int. J. Mass. Spectrom. **201**, 135 (2000).
[11] E. Herbst and Y. Osamura, Astrophys. J. **679**, 1670 (2008).
[12] N. Douguet, S. Fonseca dos Santos, M. Raoult, O. Dulieu, A. E. Orel, and V. Kokoouline, J. Chem. Phys. **142**, 234309 (2015).
[13] M. Khamesian, N. Douguet, S. Fonseca dos Santos, O. Dulieu, M. Raoult, W. J. Brigg, and V. Kokoouline, Phys. Rev. Lett. **117**, 123001 (2016).
[14] M. Khamesian, N. Douguet, S. Fonseca dos Santos, O. Dulieu, M. Raoult, and V. Kokoouline, Eur. Phys. J. D **70**, 240 (2016).
[15] F. Güthe, M. Tulej, M. V. Pachkov, and J. P. Maier, Astrophys. J. **555**, 466 (2001).
[16] T. Sommerfeld, J. Phys.: Conf. Ser. **4**, 245 (2005).
[17] F. Carelli, M. Satta, T. Grassi, and F. A. Gianturco, Astrophys. J. **774**, 97 (2013).
[18] P. D. Burrow, A. E. Howard, A. R. Johnston, and K. D. Jordan, J. Phys. Chem. **96**, 7570 (1992).
[19] T. Sommerfeld and S. Knecht, Eur. Phys. J. D **35**, 207 (2005).
[20] W. Skomorowski, S. Gulania, and A. I. Krylov, Phys. Chem. Chem. Phys. **20**, 4805 (2018).
[21] F. Sebastianelli and F. A. Gianturco, Eur. Phys. J. D **59**, 389 (2010).
[22] J. Rajput, L. Lammich, and L. H. Andersen, Phys. Rev. Lett. **100**, 153001 (2008).
[23] K. Graupner, T. A. Field, and G. C. Saunders, Astrophys. J. **685**, L95 (2008).
[24] K. J. Reed, A. H. Zimmerman, H. C. Andersen, and J. I. Brauman, J. Chem. Phys. **64**, 1368 (1976).
[25] C. M. Oana and A. I. Krylov, J. Chem. Phys. **127**, 234106 (2007).
[26] Y. Liu and C. Ning, J. Chem. Phys. **143**, 144310 (2015).
[27] L. A. Collins and B. I. Schneider, Phys. Rev. A **29**, 1695 (1984).
[28] N. Douguet, S. Fonseca dos Santos, M. Raoult, O. Dulieu, A. E. Orel, and V. Kokoouline, Phys. Rev. A **88**, 052710 (2013).
[29] T. N. Rescigno and A. E. Orel, Phys. Rev. A **25**, 2402 (1982).
[30] W. Sun, R. M. Pitzer, and C. W. McCurdy, Phys. Rev. A **40**, 3669 (1989).
[31] J. C. Light, J. Ross, and K. E. Shuler, in *Kinetic Processes in Gases and Plasmas*, edited by A. R. Hochstim (Academic, New York, 1969), pp. 281–320.
[32] G. Grell, S. I. Bokarev, B. Winter, R. Seidel, E. F. Aziz, S. G. Aziz, and O. Kühn, J. Chem. Phys. **143**, 074104 (2015).
[33] P. Duffy, D. P. Chong, M. E. Casida, and D. R. Salahub, Phys. Rev. A **50**, 4707 (1994).
[34] S. Hamel, P. Duffy, M. E. Casida, and D. R. Salahub, J. Electron Spectrosc. Relat. Phenom. **123**, 345 (2002).
[35] F. E. Harris and H. H. Michels, J. Chem. Phys. **43**, S165 (1965).
[36] H. Le Rouzo, Int. J. Quantum Chem. **64**, 647 (1997).
[37] R. A. Kendall, T. H. Dunning, and R. J. Harrison, J. Chem. Phys. **96**, 6796 (1992).
[38] I. Ema, J. M. García de la Vega, G. Ramírez, R. López, R. J. Fernández, H. Meissner, and J. Paldus, J. Comput. Chem. **24**, 859 (2003).
[39] T. N. Rescigno and A. E. Orel, Phys. Rev. A **24**, 1267 (1981).
[40] F. A. Gianturco and T. Stoecklin, J. Phys. B: At., Mol. Opt. Phys. **27**, 5903 (1994).
[41] M. A. Morrison and L. A. Collins, Phys. Rev. A **17**, 918 (1978).
[42] N. T. Padial and D. W. Norcross, Phys. Rev. A **29**, 1742 (1984).
[43] W. N. Sams and D. J. Kouri, J. Chem. Phys. **51**, 4809 (1969).
[44] W. N. Sams and D. J. Kouri, J. Chem. Phys. **51**, 4815 (1969).
[45] C. M. Oana and A. I. Krylov, J. Chem. Phys. **131**, 124114 (2009).
[46] R. G. Tonkyn, J. W. Winniczek, and M. G. White, Chem. Phys. Lett. **164**, 137 (1989).
[47] K. M. Ervin, I. Anusiewicz, P. Skurski, J. Simons, and W. C. Lineberger, J. Phys. Chem. A **107**, 8521 (2003).
[48] K. P. Huber and G. Herzberg, *Molecular Spectra and Molecular Structure: IV. Constants of Diatomic Molecules*, 1st ed. (Springer, New York, 1979).
[49] S. E. Bradforth, E. H. Kim, D. W. Arnold, and D. M. Neumark, J. Chem. Phys. **98**, 800 (1993).
[50] R. T. Wiedmann, R. G. Tonkyn, M. G. White, K. Wang, and V. McKoy, J. Chem. Phys. **97**, 768 (1992).
[51] J. R. Smith, J. B. Kim, and W. C. Lineberger, Phys. Rev. A **55**, 2036 (1997).
[52] G. Parlant and F. Fiquet-Fayard, J. Phys. B: At. Mol. Phys. **9**, 1617 (1976).

[53] L. M. Branscomb, Phys. Rev. **148**, 11 (1966).
[54] H.-J. Werner, P. J. Knowles, G. Knizia, F. R. Manby, M. Schütz, *et al.*, MOLPRO, version 2012.1, a package of *ab initio* programs, 2012; see http://www.molpro.net.
[55] R. J. Fernández, R. López, I. Ema, and G. Ramírez, J. Comput. Chem. **25**, 1987 (2004).
[56] Y. Shao, Z. Gan, E. Epifanovsky, A. T. Gilbert, M. Wormit, J. Kussmann, A. W. Lange, A. Behn, J. Deng, X. Feng, D. Ghosh, M. Goldey, P. R. Horn, L. D. Jacobson, I. Kaliman, R. Z. Khaliullin, T. Kuś, A. Landau, J. Liu, E. I. Proynov *et al.*, Mol. Phys. **113**, 184 (2015).
[57] S. Gozem and A. I. Krylov, EZDYSON Users Manual. http://iopenshell.usc.edu/downloads.
[58] S. Gozem, A. O. Gunina, T. Ichino, D. L. Osborn, J. F. Stanton, and A. I. Krylov, J. Phys. Chem. Lett. **6**, 4532 (2015).
[59] R. A. Beyer and J. A. Vanderhoff, J. Chem. Phys. **65**, 2313 (1976).
[60] D. S. Burch, S. J. Smith, and L. M. Branscomb, Phys. Rev. **112**, 171 (1958).
[61] L. C. Lee and G. P. Smith, J. Chem. Phys. **70**, 1727 (1979).
[62] S. Trippel, J. Mikosch, R. Berhane, R. Otto, M. Weidemüller, and R. Wester, Phys. Rev. Lett. **97**, 193003 (2006).
[63] P. Hlavenka, R. Otto, S. Trippel, J. Mikosch, M. Weidemüller, and R. Wester, J. Chem. Phys. **130**, 061105 (2009).
[64] I. I. Fabrikant, J. Phys. B: At., Mol. Opt. Phys. **49**, 222005 (2016).
[65] S. S. Kumar, D. Hauser, R. Jindra, T. Best, Š. Roučka, W. D. Geppert, T. J. Millar, and R. Wester, Astrophys. J. **776**, 25 (2013).
[66] W. Arbelo-González, R. Crespo-Otero, and M. Barbatti, J. Chem. Theory Comput. **12**, 5037 (2016).